Conformational Equilibration Time of Unfolded Protein Chains and the Folding Speed Limit†

Christina J. Abel,‡ Robert A. Goldbeck,*,‡ Ramil F. Latypov,§,|| Heinrich Roder,§ and David S. Kliger‡

Department of Chemistry and Biochemistry, University of California, Santa Cruz, California 95064, and Basic Science Division, Fox Chase Cancer Center, Philadelphia, Pennsylvania 19111

Received November 6, 2006; Revised Manuscript Received February 2, 2007

ABSTRACT: The speed with which the conformers of unfolded protein chains interconvert is a fundamental question in the study of protein folding. Kinetic evidence is presented here for the time constant for interconversion of disparate unfolded chain conformations of a small globular protein, cytochrome *c*, in the presence of guanidine hydrochloride denaturant. The axial binding reactions of histidine and methionine residues with the Fe(II) heme cofactor were monitored with time-resolved magnetic circular dichroism spectroscopy after photodissociation of the CO complexes of unfolded protein obtained from horse and tuna and from several histidine mutants of the horse protein. A kinetic model fitting both the reaction rate constants and spectra of the intermediates was used to obtain a quantitative estimate of the conformational diffusion time. The latter parameter was approximated as a first-order time constant for exchange between conformational subensembles presenting either a methionine or a histidine residue to the heme iron for facile binding. The mean diffusional time constant of the wild type and variants was 3 ± 2 μs, close to the folding "speed limit". The implications of the relatively rapid conformational equilibration time observed are discussed in terms of the energy landscape and classical pathway time regimes of folding, for which the conformational diffusion time can be considered a pivot point.

The earliest events in protein folding are of particular interest in understanding how an unfolded protein starts from the vast number of conformations available to it and evolves to the native fold on a physiologically useful time scale. Levinthal's paradox, which considers a worst case scenario for this problem, holds that a random search of conformational space would require astronomical amounts of time to find the folded state (*1*). Apparently much of conformational space must be kinetically or energetically inaccessible to protein sequences that are observed to fold, as folding is guided by a reaction pathway in a classical kinetic view or by funnels biasing conformational diffusion on a free energy landscape in a more general statistical mechanical view. The former view, adopted implicitly by many experimentalists, assumes that folding follows well-defined kinetic pathways that are marked by passages over transition states and perhaps involve some discrete intermediates (*2*−*6*). The latter view, introduced more recently by theorists studying formal and computational models, treats folding as a diffusional process involving conformational ensembles on a finely featured free energy landscape for which the concepts of discrete pathways and intermediates may be ill-defined (*7*−*12*).

The natural time scales of applicability of these two viewpoints may be distinguished very broadly by a parameter that has become increasingly accessible to experimental measurement: the conformational diffusion time constant of the unfolded chains, τ_d. Recent evidence suggests that τ_d is on the microsecond time scale for ∼100-residue protein chains (*13*−*17*). Given this evidence, we might expect that experimentalists looking at folding reactions proceeding on millisecond and longer time scales would find conventional kinetic thinking useful: the unfolded chain conformations will be in rapid equilibrium, averaging the heterogeneity of their detailed conformational dynamics such that the folding kinetics can be characterized simply by the thermodynamics of and passage time over a single (or perhaps a small number of) transition state free energy barrier(s). Molecular dynamics simulations of proteins, on the other hand, have generally been limited to times much less than 10^{-6} s, which may not be enough time for the unfolded ensembles to reach conformational equilibrium. Thus, the results of computer simulations of folding kinetics have tended to focus on a time regime in which we could expect that conformational diffusion biased by free energy funnels, i.e., the "new" view, might play a dominant role.

The relatively recent advent of methods improving the time resolution of folding studies beyond the limitations imposed by the mixing time of stopped-flow techniques, typically through the use of a laser pulse to trigger folding or unfolding on time scales much shorter than a millisecond (*18*−*22*), has allowed experimentalists to probe the critical early events in the folding process (*23*). Although these new developments in theoretical and experimental methods represent important milestones, relatively few studies have directly addressed the fundamental distinction between the classical and energy

† Supported by National Institutes of Health Grants EB02056 (D.S.K.) and GM056250 and CA06927 (H.R.).

* To whom correspondence should be addressed. Tel: 831-459-4007. Fax: 831-459-2935. E-mail: goldbeck@chemistry.ucsc.edu.

‡ University of California.

§ Fox Chase Cancer Center.

|| Present address: Amgen Inc., Thousand Oaks, CA 91320.

10.1021/bi0622930 CCC: $37.00
Published on Web 03/13/2007

landscape views presented by the conformational diffusion time (*13*). This situation has contributed in some part to the controversy about the validity of the new view (*24*−*26*).

The measurement of conformational diffusion in unfolded cytochrome *c* presented here used the CO photolysis method of Roder, Eaton, and co-workers to rapidly initiate folding reactions (*18*). While His-18 remains bound to the heme iron under most denaturing conditions, Met-80 dissociates readily and can be replaced by other side chains or exogenous ligands such as CO. The reduced protein is mainly folded in 4.6 M guanidine hydrochloride at 40 °C but unfolds when Met-80 is displaced by CO. Photodissociation of CO then allows Met-80 to rebind, as well as other nonnative ligands, principally His-33, His-26, or Met-65, as the protein attempts to refold. However, the time scale for rebinding of CO (∼1 ms at 1 atm of CO) limits the observational window of this method to the earliest folding events. Besides the tertiary structural features represented by heme−residue coordination, these early events also include a modest amount of helical secondary structure formation on the ∼1 μs time scale, although the ∼10% of native-like helical structure formed probably does not correspond to folding to the native state (*27*, *28*).

Motivated by the pivotal role outlined above for conformational diffusion in distinguishing different views of folding, we report here the direct measurement of the unfolded conformational diffusion time constant of a folding-competent protein sequence. We report the results of fast time-resolved magnetic circular dichroism (TRMCD) measurements for several histidine variants of cytochrome *c* after photodissociation of the denatured CO complex. A previous TRMCD study of unfolded cytochrome *c*−CO presented qualitative evidence that the conformational dynamics of the unfolded chains affected the kinetics of the microsecond time scale heme−residue binding reactions observed after CO photodissociation, an observation which suggested that the unfolded conformations were not in rapid equilibrium on this time scale (*13*). In the present study, one or both of the histidine residues (His-33, His-26) that can compete with methionine (Met-80, Met-65) for coordination to the heme as the protein attempts to refold is mutated out of the sequence. We exploit the expected overlap between the time scales for heme−residue binding and chain conformational change to deconvolute the rate of the latter process, τ_d^{-1}, from the systematic changes observed in the binding kinetics with sequence mutation. Our kinetic model, explicitly accounting for conformational equilibration of the unfolded chains, fits both the reaction rate constants and the spectra of the intermediates to obtain a quantitative estimate for the conformational diffusion time constant, a value that we compare with previous measurements of related conformational dynamics in other unfolded proteins and peptides, and to the ultimate "speed limit" for folding.

EXPERIMENTAL PROCEDURES

Sample Preparation. Horse heart and tuna heart cytochrome *c* proteins were obtained from Sigma and used without additional purification. The horse heart cytochrome *c* mutants H33N, H26Q, and H26Q/H33N were prepared following published procedures (*29*) (see also ref *30*), and mutant protein expression was confirmed with mass spectrometry. The horse H33N and H26Q/H33N mutants were prepared at FCCC. The horse H26Q mutant was prepared at UCSC from the plasmid pBRT1 (*31*, *32*). All protein samples used in the photolysis experiments were partially denatured in 4.6 M guanidine hydrochloride, pH 6.5 sodium phosphate buffer and saturated with 1.0 atm of carbon monoxide to produce nearly quantitative CO complexes with per heme concentrations of 80−90 μM.

Scheme 1: Kinetic Model for Heme−Residue Binding and Conformational Exchange Reactions of Unfolded Cytochrome *c*−CO

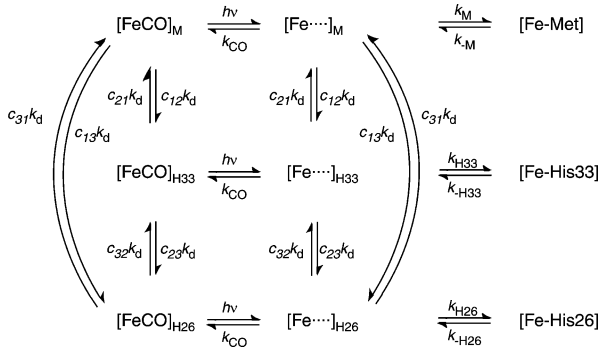

TRMCD Spectroscopy. Soret region (370−490 nm) TRMCD spectra were obtained from the Kramers−Kronig transform of time-resolved magnetic optical rotatory dispersion spectra collected at 35 logarithmic time intervals ranging from 630 ns to 6 ms after laser photolysis. The MORD spectra were averaged from 1256 to 1500 scans measured for each cytochrome *c* variant on a nanosecond laser photolysis apparatus modified for near-null polarimetry with a reference polarizer angle (β) of 0.625 deg (*33*−*35*). A matched pair of electromagnets provided oppositely oriented magnetic fields of 0.75 T for the sample and the Faraday compensator. Photolysis was initiated by 8 ns, 28 mJ, 10 mm diameter excitation pulses from a frequency-doubled Nd:YAG laser (532 nm) operated at 3.3 Hz. A microsecond xenon flashlamp probe beam was passed through the sample nearly collinear to the laser beam and detected with a spectrograph and multichannel analyzer. Protein samples were flowed through the sample cell (0.058 cm path length) to remove laser photodegradation products and ensure saturation of CO binding to the heme.

Data Analysis. The TRMCD data were arranged into an array indexed by wavelength and time for each cytochrome *c* variant, and each array was filtered using singular value decomposition (SVD) to reduce experimental noise. Each filtered data matrix, A_r, included only those spectral and temporal components corresponding to the first *r* singular values of the SVD, $r = 4$ being the effective rank of the data matrices for each of the variants studied. The filtered data matrices were then analyzed for the microscopic rate processes shown in Scheme 1 by a global analysis procedure described further below. Briefly, a gradient search was used to find the set of kinetic parameter values that minimized the sum of squares of the differences between the first *r* SVD temporal components and their best (least-squares) representation in the basis of reaction intermediate population time profiles calculated from a given set of kinetic parameter values. The details of SVD and global spectrokinetic fitting can be found in reviews (*36*−*38*). Algorithms for these procedures were written in Matlab (MathWorks).

Global Kinetic Model. Starting from the assumption that the speed of intrachain conformational diffusion is intermediate between the very rapid ($\tau_d \ll 1$ μs) and very slow ($\tau_d >$ 100 μs) scenarios used in previous studies to analyze the heme−residue binding kinetics after denatured cytochrome *c*−CO photodissociation, we applied a model (see Scheme 1) that incorporated both the multiple heme−residue binding equilibria introduced by Jones et al. (*18*) and the explicit consideration of conformational diffusion suggested by Goldbeck et al. (*13*). All binding reactions were treated as first order: k_M described the aggregate binding reaction of Met-65 and Met-80, k_{H26} and k_{H33} described the respective binding reactions of His-26 and His-33, and k_{CO} corresponded to the pseudo-first-order rate constant for CO rebinding. Separate rate constants were used for His-26 and His-33 in order to fit the different histidine variants studied. Because methionine mutants were not studied, the model did not distinguish Met-65 from Met-80 binding. Previous studies have noted that two time constants for CO rebinding are observed in phenomenological exponential fitting of absorption and MCD data for this system (*13*, *18*, *27*), which would tend to suggest the presence of additional CO rebinding intermediates (*29*). However, as discussed further below, the biphasic return of CO seemed to be well described in this study by one microscopic CO rate constant in conjunction with the multiple heme−residue equilibria of Scheme 1.

The effect of conformational diffusion was approximated by first-order rate processes for interchange between subensembles of (CO-coordinated or 5-coordinate heme) unfolded chain conformers, the latter being distinguished by the residue presented for most facile binding to the heme moiety, His-26, His-33, or a methionine: e.g., $[Fe\cdots]_{H26}$, $[Fe\cdots]_{H33}$, and $[Fe\cdots]_M$, respectively, for the 5-coordinate−heme subensembles. The rate constant k_d was multiplied in the diffusional reactions in Scheme 1 by coefficients that reflected the steady-state populations of the subensembles. For instance, $c_{ij}\,k_d$ was the rate constant for the conformational change $[Fe\cdots]_i \rightarrow [Fe\cdots]_j$ (using the numbering order: M, H33, H26), where $c_{ij} = f_j/(f_j + f_i)$ and the f_i are the fractional subpopulations of the respective subensembles. The values of f_i were estimated from the effective concentrations of the residues, which were free parameters in the modeling procedure. For example, $f_1 = [Met]_{eff}/([Met]_{eff} + [His33]_{eff} + [His26]_{eff})$.

The residue on and off rate constants were each calculated from two parameters, a binding time constant $\tau = (k_{on} + k_{off})^{-1}$ and a unimolecular binding constant $K^{uni} = k_{on}/k_{off}$. For example, the on rate constant for methionine binding was given by $k_M = [\tau_M(1 + 1/K_{Met}^{uni})]^{-1}$ and the off rate constant by $k_{-M} = [\tau_M(1 + K_{Met}^{uni})]^{-1}$. The time constants for His-26, His-33, and aggregate methionine binding were each free parameters. The unimolecular binding constants were themselves calculated from the bimolecular binding constants for histidine and methionine measured by Tezcan et al. (*39*) in microperoxidase-8, $K_{Met}^{bi} = 430\ M^{-1}$ and $K_{His}^{bi} = 1700\ M^{-1}$ (pH 7), and the effective concentrations of the respective residues. For example, $K_{Met}^{uni} = k_M/k_{-M} = [Met]_{eff}K_{Met}^{bi}$. These parametrizations had the effect of constraining the kinetic fitting procedure to reproduce the known thermodynamics of ferrocytochrome *c* heme−residue binding.

The fitting procedure was further constrained by comparing the calculated MCD spectra for reaction intermediates to model spectra (*13*). A term proportional to the sum of squares of the (calculated − model) difference spectrum for each intermediate was added to the function minimized in the fitting procedure. This spectral constraint procedure has been described previously (*40*). Four types of intermediate spectra were calculated, corresponding to the four types of heme coordination present (Scheme 1): the 6-coordinate heme species, [Fe-Met], [Fe-His], and [FeCO] and the 5-coordinate form [Fe···] (the other heme axial ligand being in all cases the proximal histidine, His-18). The corresponding model spectra were taken from ferrocytochrome *c*, ferrocytochrome b_5, and the CO complex and 5-coordinate form of cytochrome c_3, respectively (*41*, *42*).

To summarize the parametrization, a total of eight free parameters were used: k_d, k_{CO}, $[Met]_{eff}$, $[His33]_{eff}$, $[His26]_{eff}$, τ_M, τ_{H33}, and τ_{H26}. These parameters were optimized simultaneously for all five cytochrome *c* variants studied, on the assumption that the small differences in their primary sequences would not greatly affect the distribution of chain conformers and their interconversion rates, nor the inherent kinetics of heme−CO binding and the binding of residues presented quasi-geminately to the heme. With the goal of testing the assumption that k_d was independent of small sequence variations, an additional optimization was performed in which a separate k_d value was optimized for each variant while the values of the remaining free parameters were optimized simultaneously across all the variants.

RESULTS

TRMCD Spectra. The Soret band TRMCD spectra of the cytochrome *c* histidine variants shown in Figure 1 share several common features that reflected the similar evolution of heme coordination following CO photolysis in each variant. The earliest time spectrum of each variant showed a peak near 430 nm and a trough near 400 nm associated with the MCD *C* terms of paramagnetic 5-coordinate heme, the immediate product of the CO photodissociation. The last time spectrum of each variant contained a peak near 410 nm and a trough near 420 nm that together make up the *A* term of the diamagnetic CO complex, the starting material and final product of the reversible photocycle. Progressing through the intermediate time spectra, the 430 nm peak first shifted to the blue as methionine coordinated to the vacant heme site during the first several microseconds (the asymmetric *A* term of His-Fe-Met coordinated heme having a prominent peak that is blue shifted at least 10 nm from the 5-coordinate peak). Variants possessing a His-33 or His-26 residue (see panels a−d) also showed a further drop in MCD intensity over tens of microseconds as the formation of His-Fe-His (bis-His) heme coordination on this time scale was associated with the weakest MCD signal of the coordination forms present here. Finally, the return of CO coordination, present in all the variants on the hundreds of microseconds time scale, was seen most clearly in the double His mutant as a reversal in the signatures of the MCD extrema on either side of the zero crossing near 415 nm (see panel e).

SVD Components. The SVD components corresponding to the filtered data of Figure 1 are shown in Figure 2. For all variants, the largest component (V_1) decayed modestly

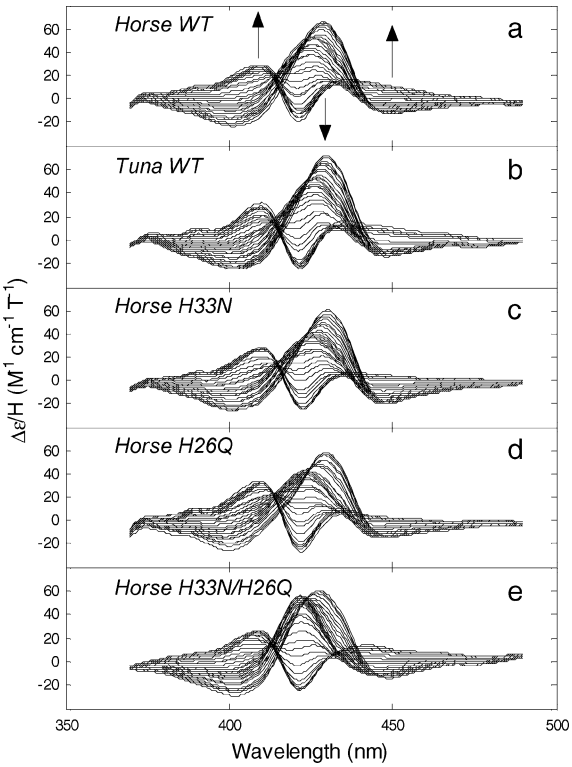

FIGURE 1: TRMCD spectra (SVD filtered) measured after CO photodissociation from denatured cytochrome *c* proteins: wild type (a) horse and (b) tuna and horse mutants (c) H33N, (d) H26Q, and (e) H33N/H26Q at 40 °C, pH 6.5, in 4.6 M guanidine hydrochloride. Arrows (panel A) indicate the direction of time, starting at 600 ns and ending at 6 ms.

in amplitude on the residue binding time scale, 1−100 μs, and then lost most of its amplitude on the CO rebinding time scale, 100−1000 μs. The corresponding U_1 spectra thus represent the average spectral amplitudes of the TRMCD spectra taken at times before about 100 μs, which are centered between 420 and 430 nm. Comparing the lower with the upper panels of Figure 2, the effect of removing one or both of the histidine residues that can bind to the distal heme site is seen mainly as a smaller decay in the amplitude of V_1 over the first 100 μs, as well as a smaller rise in the amplitude of V_2 between 10 and 100 μs. The evolution of V_3 below 10 μs, which shows a modest increase in amplitude as the histidines are removed, appears to reflect mainly the binding of methionine on this time scale. Its retrograde evolution after 100 μs corresponds with the return of CO ligation. Finally, the weighted amplitude of V_4 was quite small, consistent with the assumption that the SVD components V_i for $i > 4$ can be neglected as experimental noise.

The principal utility of the SVD procedure, besides filtering noise, was in reducing the data to a compact set of model-independent spectrally global time evolution traces for kinetic modeling, as explained in Experimental Procedures. The quality of the fits derived from the model in Scheme 1 to the SVD time evolutions observed for the cytochrome *c* variants was very good (see Figure 2), suggesting that the model indeed provided a good representation of the experimental dynamics. However, the mathematical orthogonality of the SVD components tended to mix within them the contributions of different physical intermediates. To gain better insight into the latter, we turned to the calculated spectra and time evolutions of the reaction intermediates shown in Figure 3.

Calculated Spectra and Time Courses of Intermediates in Scheme 1. The shapes and magnitudes of the calculated spectra (Figure 3a−e) were in reasonable agreement with the corresponding model spectra (Figure 4) given that the samples studied were denatured whereas the model spectra were taken from native proteins. The high-spin pentacoordinate heme species [Fe•••], possessing the characteristically strong MCD peak near 430 nm seen in the corresponding model spectrum, decayed initially via binding of Met-65 or Met-80 to form the diamagnetic species [Fe-Met] (Figure 3f−j) with a time constant of ∼1 μs (Table 1). The latter species was calculated for each protein variant to have an MCD peak that was blue shifted by 10 nm from that of [Fe•••], consistent with the corresponding peak shift between the pentacoordinate and His-Fe-Met model spectra. The fast Met binding process was followed by the slower binding of His-26 or His-33 to form diamagnetic [Fe-His] with time constants of ∼60 and ∼30 μs, respectively (see Table 1). The calculated spectra of the latter species in each variant resembled the corresponding model spectrum in having a weak positive MCD band near the absorption band maximum at ∼425 nm that was flanked on either side by MCD troughs. The aggregate amplitude of the histidine binding processes in tuna WT and the single-His horse mutants was about half that of the horse WT, consistent with the difference in overall histidine binding stoichiometry and the similar effective concentrations (and unimolecular binding rate constants) calculated for the His-26 and His-33 residues. Given the similar aggregate effective concentrations for methionine and histidine residues observed here (see Table 1), the significantly slower binding of histidines compared with methionines observed in Figure 3 can be assigned mainly to the slower intrinsic bimolecular binding rate constants, k'_{H33} and k'_{H26}, of the former species. The formation of final product for each variant in Figure 3, [Fe-CO], was described by a single microscopic rate constant of ∼(200 μs)$^{-1}$. Previous studies have noted the apparently biphasic nature of CO recombination in this system, and indeed two-exponential fits of the CO return curves in Figure 3 (results not shown) reproduced the ∼100 and ∼1000 μs time constants reported before (*18*, *27*, *29*). However, the ability of Scheme 1 to describe this aspect of the kinetics in terms of a single CO binding rate constant suggests that the presence of back-reactions in the multiple heme−residue binding reactions competing with CO rebinding probably explains the observation of two apparent recombination rates, rather than the presence of additional CO binding intermediates.

Conformational Diffusion of Unfolded Chains. By approximating the complex diffusional processes through which the unfolded chain conformations are expected to evolve in a statistical mechanical picture by the simple first-order rate processes shown in Scheme 1, the influence of conformational diffusion on the observed heme−residue binding kinetics was deconvoluted in a fitting procedure applied to the data for all the protein variants simultaneously. This procedure yielded a global diffusion time constant, $\tau_d = 1/k_d \approx 3$ μs (see Table 1). Applying a similar fitting procedure that varied the individual τ_d values of the variants as free parameters yielded values of 7.6, 5.4, 2.8, 2.5, and 1.4 μs for horse WT, tuna WT, horse H33N, horse H26Q, and horse

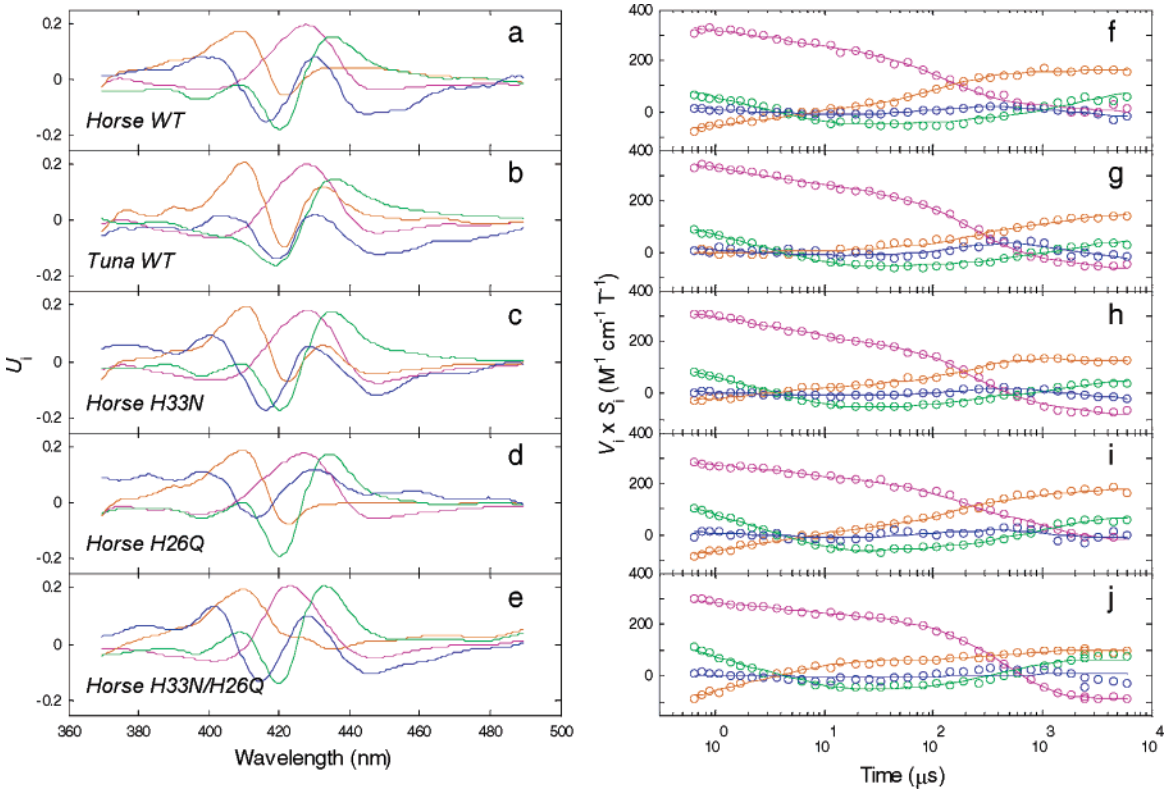

FIGURE 2: SVD components $i = 1$, 2, 3, and 4 (magenta, orange, green, and blue), corresponding to the TRMCD data for cytochrome *c* variants shown in Figure 1. Orthonormal spectral components U_i for (a) horse wild type, (b) tuna wild type, (c) horse H33N mutant, (d) horse H26Q mutant, and (e) horse H33N/H26Q double mutant, and (f−j) the respective orthonormal temporal components V_i multiplied by their singular values S_i. Lines in panels f−j show the fits to experimental points (○) calculated from the kinetic model (Scheme 1).

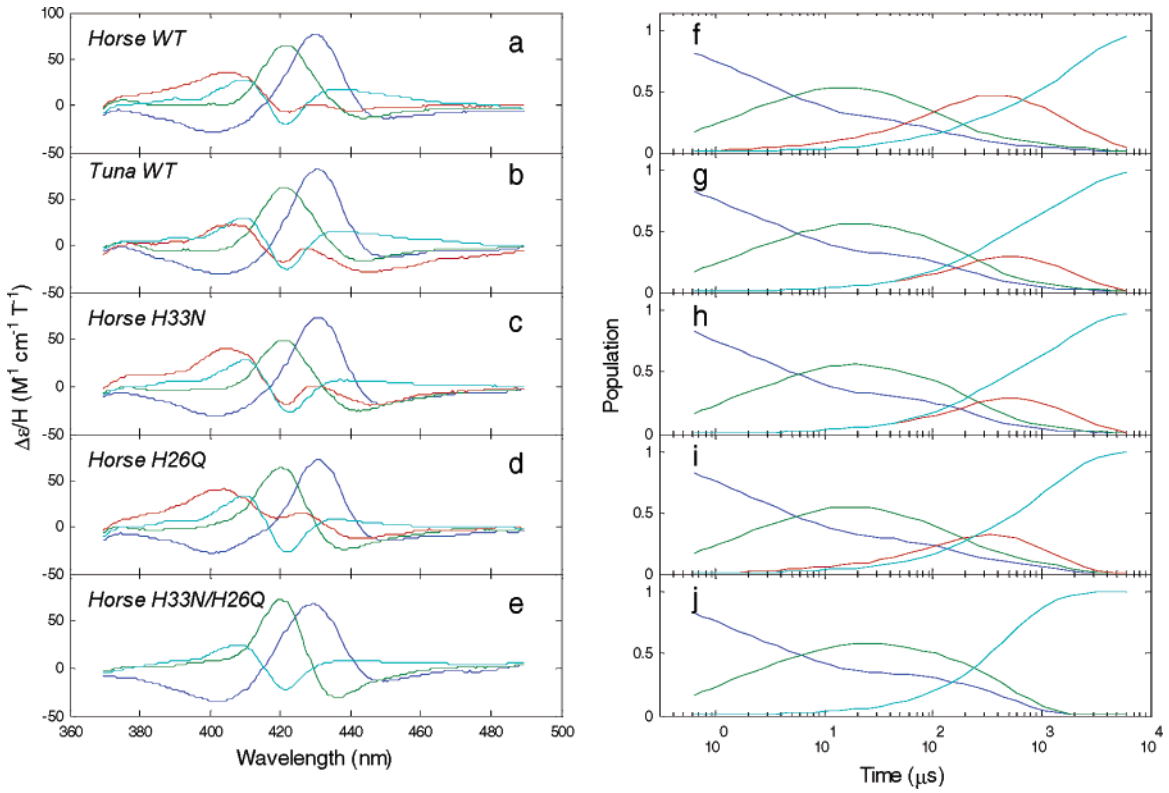

FIGURE 3: Calculated MCD spectra and time courses of heme-coordination reaction intermediates: [Fe···] (blue), [Fe-Met] (green), [Fe-His] (red), and [FeCO] (cyan). Cytochrome *c* variant panels are labeled as in the Figure 1 legend.

H33N/H26Q, respectively, while returning values for the remaining free parameters that were very similar to those obtained from the fitting procedure that used a global τ_d value. The rather close distribution of individual variant τ_d values around the global τ_d value supports the assumption that small differences in the primary sequences of the variants

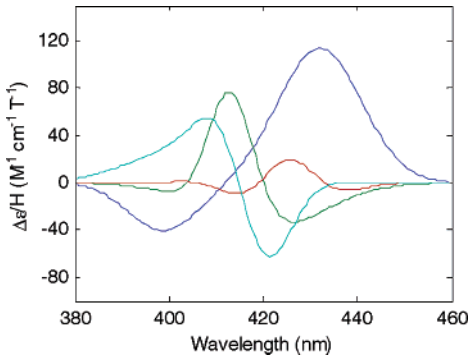

FIGURE 4: Model MCD spectra for 5-coordinate (blue), His-Fe-Met (green), His-Fe-His (red), and His-Fe−CO (cyan) heme species, taken from photolyzed cytochrome c_3−CO, ferrocytochrome *c*, ferrocytochrome b_5, and cytochrome c_3−CO, respectively.

Table 1: Kinetic Parameters from Scheme 1 Optimized Simultaneously for Data from Cytochrome *c* Horse and Tuna Wild Types and Horse H33N, H26Q, and H33N/H26Q Mutants[a]

k_d	$3.4 \times 10^5\ s^{-1}$	k_M	$1.2 \times 10^6\ s^{-1}$
k_{CO}	$5.5 \times 10^3\ s^{-1}$	k_{H33}	$3.5 \times 10^4\ s^{-1}$
τ_M	0.85 μs	k_{H26}	$1.7 \times 10^4\ s^{-1}$
τ_{H33}	28 μs	k_{-M}	$3.0 \times 10^5\ s^{-1}$
τ_{H26}	59 μs	k_{-H33}	$3.5 \times 10^3\ s^{-1}$
[Met]	9.2 mM	k_{-H26}	$1.4 \times 10^3\ s^{-1}$
[His33]	5.9 mM	k'_M	$1.3 \times 10^8\ M^{-1}\ s^{-1}$
[H26]	6.9 mM	k'_{H33}	$5.9 \times 10^6\ M^{-1}\ s^{-1}$
		k'_{H26}	$2.5 \times 10^6\ M^{-1}\ s^{-1}$

[a] Parameter uncertainties are within ±10% except for k_d, which is ±50%.

did not have a large effect on the broad measure of conformational diffusion represented by τ_d.

The τ_d value reported here was on a time scale intermediate between completely frozen ($\tau_d \gg \tau_M$, τ_{H33}, τ_{H26}) and completely free ($\tau_d \ll \tau_M$, τ_{H33}, τ_{H26}) conformational equilibration, as anticipated. However, this time scale was rapid enough that the effects of conformational diffusion on the observed binding kinetic results were found to be rather subtle. An alternative fitting procedure that kept τ_d fixed at a sufficiently small value, 10 ns, that we would expect no influence on the residue binding kinetics produced results (not shown) that were similar to those reported for the optimized τ_d fitting procedure except that τ_M roughly doubled in length to 2 μs, the small negative lobe near 420 nm in the calculated MCD spectrum of the [Fe-His] species became more positive in value for each of the histidine-containing variants, and the value of χ^2 increased by 5%, i.e., the quality of the fits decreased. The statistical significance of the improvement in fit quality obtained with the addition of τ_d as a fitting parameter was supported by the high statistical power of the data (132 degrees of freedom), allowing us to discard the hypothesis that the improvement came from the fitting of random noise. Applying the *F*-statistic test, we obtained an F_χ value of 8, giving us greater than 99% confidence in the physical significance of the conformational diffusion rate constant, $k_d = 1/\tau_d$, used in Scheme 1 (*43*).

DISCUSSION

The kinetics of cytochrome *c*'s early folding events [comprising rapid helical folding reactions (*27*, *28*), chain collapse (*44*, *45*), and in the case of the CO photolysis system, heme−residue binding reactions (*18*)] have been investigated previously for evidence of slow conformational diffusion in the unfolded chains (*13*, *15*, *16*, *28*, *46*). Hagen et al. (*16*) measured the bimolecular rate constant for the binding of free methionine to nearly unhindered heme in microperoxidase ($2 \times 10^8\ M^{-1}\ s^{-1}$) and noted that multiplying this rate by the Jacobson−Stockmayer factor for heme−Met-80 contact in denatured cytochrome *c* (~1 mM) yielded an estimate for the unimolecular binding rate constant, $(5\ \mu s)^{-1}$, that was much faster than the $(40\ \mu s)^{-1}$ rate constant assigned to heme−Met binding in the unfolded protein by Jones et al. (*18*). [The Jacobson−Stockmayer factor is essentially a rough estimate, based on random polymer statistics, of the effective concentration of the Met-80 residue at the heme site in unfolded cytochrome *c* (*47*, *48*). In calculating the factor $[3/(2\pi C_n n l^2)]^{3/2}$, Hagen et al. assumed that the Flory characteristic ratio $C_n \approx 8$, the value observed in 6 M GuHCl (*49*), that the peptide segment length $l = 3.8$ Å, and that $n = 62$ for the heme-Met-80 loop.] They attributed the slower binding reported by Jones et al. in the protein compared with their prediction from free methionine−heme binding to the rate-limiting intrachain conformational diffusion of Met-80 to the heme site and applied an approximate steady-state diffusion expression to the results of the kinetic analysis of Jones et al. to deconvolute a 34−40 μs range for the time constant of this intrachain diffusion process.

A previous TRMCD study of this system also observed qualitative evidence for slow conformational diffusion (*13*). That study found that a kinetic analysis that used a mechanism that explicitly accounted for interchange between disparate unfolded conformers, similar to Scheme 1, gave a better fit to the MCD spectrum of the bishistidine heme-coordinated intermediate than was possible with a model that did not explicitly include conformational diffusion. That observation suggested that conformational diffusion in the unfolded chains was not significantly faster than the time scale of the residue binding reactions (3−50 μs), raising the possibility that the early folding events proceeded along multiple pathways that were kinetically separated by the many small barriers associated with the conformational dynamics of the unfolded main chain and its side chains considered as a heteropolymer. Further support for such an energy landscape view of the early folding events in cytochrome *c* came from nanosecond time scale far-UV ORD (optical rotatory dispersion) measurements that used a photoreduction trigger for folding developed by the Gray group (*22*) to probe the early formation of helical secondary structure. Chen et al. (*28*, *46*) found kinetic evidence suggesting that this microsecond time scale process proceeded within a subensemble of the unfolded chains that was kinetically isolated from the bulk of the unfolded chains on time scales up to that of the bulk photoreduction process ($t_{1/2}$ ~5 μs).

The time scale for conformational diffusion reported here for unfolded cytochrome *c* represented an aggregate of the various intrachain diffusion processes underlying the transitions between conformational subensembles included in Scheme 1, specifically the intrachain diffusion of Met-80, Met-65, His-33, and His-26 to and from the immediate vicinity of the heme moiety. Given the strong overlap of the measured τ_d value with the time scale of methionine binding, we expect that the intrachain diffusion of those

residues in particular made the strongest contribution to the aggregate measurement. In that light, our τ_d value seems surprisingly short compared with the time constant for Met−heme intrachain diffusion reported in earlier absorption studies (*16*). However, it is consistent with more recent experimental evidence from cytochrome *c* and other proteins and peptides (*14*, *15*, *17*). A 15-residue loop diffusion time constant of 250 ns was obtained from electron transfer rates measured in an unfolded $Ru(NH_3)_5^{3+}$-modified Zn-substituted cytochrome *c* (*15*). Extrapolating that value to a 62-residue loop corresponding to heme−Met-80 binding by using the $n^{1.5}$ dependence predicted from a simple ideal polymer model (*50*) gives a time constant of ∼2 μs, which is more in line with the global τ_d value reported here. However, both the ambiguity inherent in assigning a residue *n* value to the electron transfer system and the likelihood that the *n* dependence exponent is greater than 1.5 in real proteins and polypeptides contribute to the uncertainty in such an extrapolation. Krieger et al. (*17*) used triplet−triplet energy transfer to measure the end-to-end diffusion rates in a series of nonfolding Xaa-Ser repeat polypeptides of increasing length, up to a maximum of 56 residues. They found that the length dependence of the contact time scaled with an *n* exponent of 1.7 for Xaa = Gly, indicating that intramolecular interactions [principally excluded volume effects (*50*)] led to slower diffusion with increasing chain length than expected in an ideal random-walk polymer. They also found that intrachain diffusion rates varied with amino acid content and solvent: contact rate constants were roughly half as fast for polypeptides with Xaa = Ala, Ser, Glu, Arg, His, and Ile compared with Gly and were also half as fast in 4 M GuHCl compared with water. These considerations suggest that a 62-residue unfolded protein chain of varied amino acid content, corresponding to the heme−Met-80 loop, could reasonably be extrapolated from Krieger et al.'s reported rate constant of 7×10^6 s^{-1} for a 56-residue $(Gly\text{-}Ser)_x$ polypeptide to have an end-to-end conformational diffusion time constant of ∼1 μs in 4 M GuHCl. The probable barrier to intrachain diffusion presented by the covalently attached heme moiety in cytochrome *c* and the difference in temperature (22.5 vs 40 °C) between the polypeptide measurements and the present experiments prevent a direct comparison of the two results, but the similarity of τ_d and the time constant extrapolated from the polypeptide study suggest that the conformational diffusion rates of nonfolding and folding-competent peptide sequences are roughly similar.

A comparison with a conformational diffusion rate constant for another folding-competent sequence can be found in Yang and Gruebele's *T*-jump unfolding study of the λ-repressor fragment λ_{6-85} (*14*). They report a "molecular time scale" of 2 μs for fast-folding mutants of this protein, that value representing the time constant for conformational diffusion from the transition state of this two-state folder back to the unfolded state when the temperature is quickly jumped up. Their molecular time scale is complementary to the parameter τ_d reported here in the sense that the former represents the equilibration time constant between an unfolded state and a folding transition state whereas the latter reflects the equilibration time constant for the many conformers of the unfolded state of a protein. The validity of transition state theory, and thus classical pictures of folding, requires that both equilibration times be rapid compared to the overall time required for folding. Both types of equilibration times are thus crucial to distinguishing classical vs energy landscape folding scenarios for a given protein. Therefore, it is interesting that these complementary measures of conformational diffusion seem to converge so closely for different unfolded (folding-competent) chains of roughly similar residue lengths. This convergence suggests that both types of equilibration processes may not be very sensitive to the details of protein primary structure and thus that it may be possible to establish simple criteria for distinguishing classical vs nonclassical folding scenarios for single protein domains. Of course, it is difficult to generalize from the data for essentially only two wild-type sequences, cytochrome *c* and λ_{6-85}, but this view is further supported by the apparent convergence with the nonfolding polypeptide results cited above. Strikingly, these different measures of conformational diffusion times now available for unfolded chains, obtained from both folding and nonfolding sequences, appear to converge at the same value, ∼1 μs, for $n = 60-100$. Such a relatively weak dependence of the diffusion time of an unfolded protein on the nature of its primary sequence would be consistent with Krieger et al.'s polypeptide results, which suggest that the amino acid content might contribute at most a factor of 2−3 to τ_d and that its most important dependence is that on sequence length, $\tau_d \sim n^{1.7}$, much as would be expected for a random polymer with excluded volume effects.

The significantly slower estimate of intrachain diffusion reported previously for cytochrome *c* (*16*) was based on an assignment of the unimolecular rate constant for methionine binding, $(40\ \mu s)^{-1}$ (*18*), that was much slower than the value reported here, $(1-2\ \mu s)^{-1}$. The difference in the two assignments of binding rate appears to arise mainly from the different constraints applied during the respective kinetic fitting procedures. Previous absorption studies, attempting to distinguish the overlapping evolution of several 6-coordinated heme species that have similar absorption spectra (His-Fe-CO, Met-Fe-His, and His-Fe-His), used procedures that did not constrain the intensive spectra (extinction coefficients) of the intermediates (*18*, *29*). Those procedures yielded unimolecular equilibrium constants for the binding of methionine and histidine residues to the heme, $K_{Met}^{uni} = 0.1$ and $K_{His}^{uni} = 0.4$, respectively, that implied incomplete equilibrium binding of these residues in the denatured protein. In contrast, the present MCD study found equilibrium constants of 4 and 10−12 for methionine and histidine binding, respectively, from a fitting procedure that constrained the intensive intermediate spectra. This constraint was made practicable here by the much larger differences between the MCD spectra of the heme-coordination species than was observed in their absorption spectra. The larger unimolecular equilibrium constants in the present study imply nearly complete binding of protein residues to the distal heme site at equilibrium and significantly more extensive binding during the photocycle than calculated by Jones et al. (*18*). Because both the absorption studies and the current MCD study measured very similar observed time constants for methionine binding (2−4 μs), the difference in the microscopic on rates must come from this difference in the equilibrium binding constants from which the on rates were calculated. The larger unimolecular equilibrium constants for methionine and histidine binding used in the present work

were calculated as the product of the fitted effective concentrations of the residues and published bimolecular binding constants, as noted above. There do not appear to be independent measurements of the effective concentration of methionine under these conditions, but the random polymer considerations mentioned above for Met-80 concentration suggest that the total effective concentration of Met-80 and Met-65 is several millimolar, which is reasonably consistent with the 9 mM concentration found here given the approximate nature of the Jacobson−Stockmayer factors as concentration estimates. Thus the greater than unity value of the unimolecular methionine binding constant used here seems consistent with the behavior expected for these residues in a randomly configured polymer. The concentrations reported here for His-33 and His-26 were also consistent with results reported previously for this protein under denaturing conditions, 3−8 mM (*29*, *51*), and with the range expected from the Jacobson−Stockmayer factors for His-33 and His-26, 7−19 mM (using the assumptions noted above for C_n and l for Met-80 and $n = 15$ and 8 for His-33 and His-26, respectively), which tends to support the validity of the high unimolecular binding constants calculated here for these residues as well.

Although the absorption spectra of the various heme coordination species generated during the cytochrome *c*−CO photocycle are fairly similar, more definitive information about heme coordination can be obtained from their more distinctive MCD spectra (*13*). Accordingly, more direct evidence about the extent of residue binding was found in MCD denaturant titration measurements, which indicated essentially complete binding of a methionine or histidine residue at the distal site of the reduced protein at all GuHCl concentrations studied (0−6 M) in the wild type and H33N/H26Q double mutant (*52*, *53*), i.e., $K_{\mathrm{Met}}^{\mathrm{uni}} \gg 1$ and $K_{\mathrm{His}}^{\mathrm{uni}} \gg 1$, in agreement with the present results. The uniqueness of the fitted equilibrium constant values reported here was further supported by the reasonable fit of the calculated MCD extinction coefficients of the intermediates to those of the model spectra. In contrast, attempts to fit the spectrokinetic data while holding the unimolecular equilibrium binding constants fixed at the values of Jones et al. yielded MCD extinction coefficients for the [His-Fe-Met] and [His-Fe-His] intermediates that were unreasonably large (results not shown).

We now have several converging lines of evidence about the role of intrachain conformational dynamics of the unfolded state in protein folding: The equilibration time between disparate unfolded chain conformations measured in the present work for cytochrome *c* under favorable folding conditions, the molecular time scale in λ repressor fragment unfolding (*14*), and extrapolations of the end-to-end diffusion times of nonfolding peptide sequences (*17*) and the Ru- to Zn-porphyrin contact rate in denatured $Ru(NH_3)_5$(His-33)-Zn-cytochrome *c* (*15*) all suggest that the unfolded chains of 60−100 residue proteins reach conformational equilibrium with a time constant of ∼1 μs. This time scale seems remarkably independent of whether one is measuring intrachain spatial diffusion between specific contact points (*15*, *17*), more global diffusion between conformational ensembles distinguished by the target points of tertiary contact (present work), or conformational diffusion of thermally activated unfolded chains back from the folding transition state region (*14*). Moreover, the work of Krieger et al. (*17*) suggests that this time scale, while modestly sensitive to sequence composition and denaturant concentration, depends most importantly on sequence length, varying as $\tau \sim n^{1.8-2.0}$, much as would be expected for an ideal polymer ($\tau \sim n^{3/2}$). A similar asymptotic length dependence was reported in earlier work on polypeptides with lengths up to $n = 19$ by Lapidus et al. (*54*).

Together, these results support the proposal that this time scale represents a type of kinetic limit for folding in that any faster folding would not meet the prerequisite for a classical transition state theory (TST) picture, namely, that the unfolded state(s) and transition state be in conformational equilibrium. Faster folding would therefore better correspond to a downhill folding scenario in an energy landscape picture (*12*, *13*, *55*). Representing in this sense a speed limit for classical TST folding, the rate of conformational diffusion thus provides the natural prefactor $\nu \sim (1\ \mu\mathrm{s})^{-1}$ for the TST expression for folding rates, $k_f = \nu e^{-\Delta G^{\ddagger}/kT}$, in proteins of $n \sim 100$, as proposed previously by Yang and Gruebele (*14*). As those authors point out, the prefactor used for TST kinetics in small molecules, $\nu = kT/h \approx (200\ \mathrm{fs})^{-1}$, is clearly too fast to apply to protein folding. The fastest elementary secondary and tertiary structure formation events, short segment α-helical hydrogen bonding and small loop formation ($n < 10$), occur in about 10−100 ns, 5−6 orders of magnitude slower than the fastest elementary events in small molecule reactions (*56*, *57*). That observation has motivated the search for a slower prefactor appropriate to folding. One such example is the value $(100\ \mathrm{ps})^{-1}$ proposed by Pascher (*58*) on the basis of theoretical estimates of the time required to add another residue to the end of an existing helical region (*59*). However, the latter value would still be faster than the rate at which the unfolded reactant states and the folding transition state reach equilibrium, $1/\tau_d$, by several orders of magnitude. The most natural estimate of the average time required for an unfolded conformation to evolve to a transition state conformation seems to be provided by the unfolded chain conformational diffusion time, τ_d, which leads to $\nu = 1/\tau_d$ as a natural choice for the transition state prefactor. This conclusion is further supported by theoretical estimates of the folding prefactor, based on Kramers' theory for diffusion across the transition state region, which have yielded values for $1/\nu$ of ∼1−10 μs for proteins with $n \approx 80$ (*60*−*62*) [see also the review by Kubelka et al. (*55*)].

Establishing the proper prefactor for folding is necessary in order to deduce free energies of activation from the rate constants measured for the many protein folding systems that appear to follow classical TST kinetics. The temperature dependence of folding rate constants can already be measured to obtain enthalpies of activation, although non-Arrhenius behavior often introduces ambiguity into such measurements (*10*, *12*, *58*). Nevertheless, fixing the TST prefactor at a physically reasonable value would permit the assignment of unique free energies, which in turn could be combined with activation enthalpies to calculate the entropy of activation, $\Delta S^{\ddagger} = (\Delta H^{\ddagger} - \Delta G^{\ddagger})/T$. The latter quantity is of particular interest from the point of view of evaluating the Levinthal paradox in that it contains the protein's internal entropic barrier to folding, along with an important contribution from the entropy change of the solvent (*63*). Thus, determining the TST prefactor for folding is an important step toward

experimentally assessing the difficulty of the conformational search required for folding, i.e., the relative sizes of the unfolded and transition state conformational spaces of real proteins.

If $1/\tau_d$ represents the limiting rate for TST folding, it nonetheless appears to be slower in small to moderate sized proteins than the fastest possible folding events. Whereas τ_d is expected to range from microseconds to tens of microseconds for proteins with $n = 100-400$ (using the extrapolation of τ_d to larger n described above), formation of the simplest elements of secondary and tertiary structure on the 10−100 ns time scale represents a type of ultimate speed limit for folding. The observed values of these two types of limits suggest that the time regime within which experimentalists are most likely to observe the type of downhill folding processes predicted from the energy landscape perspective extends over about 3 decades of dynamic range, from 10^{-8} to 10^{-5} s, whereas folding events occurring after $\sim 10^{-5}$ s probably correspond to crossings over the more global (cooperative) free energy barriers familiar from the TST picture of protein folding.

ACKNOWLEDGMENT

We thank George McLendon for providing the plasmid pBRT1.

REFERENCES

1. Levinthal, C. (1968) Are there pathways for protein folding?, *J. Chem. Phys. 65*, 44−45.
2. Creighton, T. E. (1990) Protein folding, *Biochem. J. 270*, 1−16.
3. Kim, P. S., and Baldwin, R. L. (1990) Intermediates in the folding reactions of small proteins, *Annu. Rev. Biochem. 59*, 631−660.
4. Englander, S. W., and Mayne, L. (1992) Protein folding studied using hydrogen-exchange labeling and two-dimensional NMR, *Annu. Rev. Biophys. Biomol. Struct. 21*, 243−265.
5. Fersht, A. (1999) *Structure and Mechanism in Protein Science*: *A Guide to Enzyme Catalysis and Protein Folding*, W. H. Freeman, New York.
6. Roder, H., Maki, K., and Cheng, H. (2006) Early events in protein folding explored by rapid mixing methods, *Chem. Rev. 106*, 1836−1861.
7. Bryngelson, J. D., and Wolynes, P. G. (1987) Spin glasses and the statistical mechanics of protein folding, *Proc. Natl. Acad. Sci. U.S.A. 84*, 7524−7528.
8. Bryngelson, J. D., and Wolynes, P. G. (1989) Intermediates and barrier crossing in a random energy-model (with applications to protein folding), *J. Phys. Chem. 93*, 6902−6915.
9. Dill, K. A., and Chan, H. S. (1997) From Levinthal to pathways to funnels, *Nat. Struct. Biol. 4*, 10−19.
10. Chan, H. S., and Dill, K. A. (1998) Protein folding in the landscape perspective: chevron plots and non-Arrhenius kinetics, *Proteins: Struct., Funct., Genet. 30*, 2−33.
11. Leopold, P. E., Montal, M., and Onuchic, J. N. (1992) Protein folding funnels: a kinetic approach to the sequence-structure relationship, *Proc. Natl. Acad. Sci. U.S.A. 89*, 8721−8725.
12. Bryngelson, J. D., Onuchic, J. N., Socci, N. D., and Wolynes, P. G. (1995) Funnels, pathways, and the energy landscape of protein folding: a synthesis, *Proteins 21*, 167−195.
13. Goldbeck, R. A., Thomas, Y. G., Chen, E., Esquerra, R. M., and Kliger, D. S. (1999) Multiple pathways on a protein-folding energy landscape: kinetic evidence, *Proc. Natl. Acad. Sci. U.S.A. 96*, 2782−2787.
14. Yang, W. Y., and Gruebele, M. (2003) Folding at the speed limit, *Nature 423*, 193−197.
15. Chang, I. J., Lee, J. C., Winkler, J. R., and Gray, H. B. (2003) The protein-folding speed limit: intrachain diffusion times set by electron-transfer rates in denatured $Ru(NH_3)_5$(His-33)-Zn-cytochrome *c*, *Proc. Natl. Acad. Sci. U.S.A. 100*, 3838−3840.
16. Hagen, S. J., Hofrichter, J., Szabo, A., and Eaton, W. A. (1996) Diffusion-limited contact formation in unfolded cytochrome *c*: estimating the maximum rate of protein folding, *Proc. Natl. Acad. Sci. U.S.A. 93*, 11615−11617.
17. Krieger, F., Fierz, B., Bieri, O., Drewello, M., and Kiefhaber, T. (2003) Dynamics of unfolded polypeptide chains as model for the earliest steps in protein folding, *J. Mol. Biol. 332*, 265−274.
18. Jones, C. M., Henry, E. R., Hu, Y., Chan, C. K., Luck, S. D., Bhuyan, A., Roder, H., Hofrichter, J., and Eaton, W. A. (1993) Fast events in protein folding initiated by nanosecond laser photolysis, *Proc. Natl. Acad. Sci. U.S.A. 90*, 11860−11864.
19. Ballew, R. M., Sabelko, J., and Gruebele, M. (1996) Observation of distinct nanosecond and microsecond protein folding events, *Nat. Struct. Biol. 3*, 923−926.
20. Williams, S., Causgrove, T. P., Gilmanshin, R., Fang, K. S., Callender, R. H., Woodruff, W. H., and Dyer, R. B. (1996) Fast events in protein folding: helix melting and formation in a small peptide, *Biochemistry 35*, 691−697.
21. Munoz, V., Thompson, P. A., Hofrichter, J., and Eaton, W. A. (1997) Folding dynamics and mechanism of β-hairpin formation, *Nature 390*, 196−199.
22. Pascher, T., Chesick, J. P., Winkler, J. R., and Gray, H. B. (1996) Protein folding triggered by electron transfer, *Science 271*, 1558−1560.
23. Fersht, A. R. (1997) Nucleation mechanisms in protein folding, *Curr. Opin. Struct. Biol. 7*, 3−9.
24. Laurents, D. V., and Baldwin, R. L. (1998) Protein folding: matching theory and experiment, *Biophys. J. 75*, 428−434.
25. Pande, V. S., Grosberg, A. Y., Tanaka, T., and Rokhsar, D. S. (1998) Pathways for protein folding: is a new view needed?, *Curr. Opin. Struct. Biol. 8*, 68−79.
26. Xu, Y., Mayne, L., and Englander, S. W. (1998) Evidence for an unfolding and refolding pathway in cytochrome *c*, *Nat. Struct. Biol. 5*, 774−778.
27. Chen, E., Wood, M. J., Fink, A. L., and Kliger, D. S. (1998) Time-resolved circular dichroism studies of protein folding intermediates of cytochrome *c*, *Biochemistry 37*, 5589−5598.
28. Chen, E., Goldbeck, R. A., and Kliger, D. S. (2003) Earliest events in protein folding: submicrosecond secondary structure formation in reduced cytochrome *c*, *J. Phys. Chem. A 107*, 8149−8155.
29. Hagen, S. J., Latypov, R. F., Dolgikh, D. A., and Roder, H. (2002) Rapid intrachain binding of histidine-26 and histidine-33 to heme in unfolded ferrocytochrome *c*, *Biochemistry 41*, 1372−1380.
30. Rumbley, J. N., Hoang, L., and Englander, S. W. (2002) Recombinant equine cytochrome *c* in *Escherichia coli*: high-level expression, characterization, and folding and assembly mutants, *Biochemistry 41*, 13894−13899.
31. Pollock, W. B., Rosell, F. I., Twitchett, M. B., Dumont, M. E., and Mauk, A. G. (1998) Bacterial expression of a mitochondrial cytochrome *c*. Trimethylation of lys72 in yeast iso-1-cytochrome *c* and the alkaline conformational transition, *Biochemistry 37*, 6124−6131.
32. Rosell, F. I., and Mauk, A. G. (2002) Spectroscopic properties of a mitochondrial cytochrome *c* with a single thioether bond to the heme prosthetic group, *Biochemistry 41*, 7811−7818.
33. Esquerra, R. M., Goldbeck, R. A., Kim-Shapiro, D. B., and Kliger, D. S. (1998) Fast time resolved magnetic optical rotatory dispersion measurements. 1. Mueller analysis of optical and photoselection-induced artifacts, *J. Phys. Chem. A 102*, 8740−8748.
34. Esquerra, R. M., Goldbeck, R. A., Kim-Shapiro, D. B., and Kliger, D. S. (1998) Fast time resolved magnetic optical rotatory dispersion measurements. 2. Confirmation of Mueller analysis and application to myoglobin ligand photolysis, *J. Phys. Chem. A 102*, 8749−8758.
35. Goldbeck, R. A., Kim-Shapiro, D. B., and Kliger, D. S. (1997) Fast natural and magnetic circular dichroism spectroscopy, *Annu. Rev. Phys. Chem. 48*, 453−479.
36. Goldbeck, R. A., and Kliger, D. S. (1993) Nanosecond time-resolved absorption and polarization dichroism spectroscopies, *Methods Enzymol. 226*, 147−177.
37. Henry, E. R., and Hofrichter, J. (1992) Singular value decomposition: application to the analysis of experimental data, *Methods Enzymol. 210*, 129−192.
38. Goldbeck, R. A., and Kliger, D. S. (2001) Transient kinetic studies, in *Encyclopedia of Chemical Physics and Physical Chemistry* (Moore, J. H., and Spencer, N. D., Eds.) pp 2637−2656, IOP Publishing, Bristol.
39. Tezcan, F. A., Winkler, J. R., and Gray, H. B. (1998) Effects of ligation and folding on reduction potentials of heme proteins, *J. Am. Chem. Soc. 120*, 13383−13388.

40. Goldbeck, R. A., Esquerra, R. M., Holt, J. M., Ackers, G. K., and Kliger, D. S. (2004) The molecular code for hemoglobin allostery revealed by linking the thermodynamics and kinetics of quaternary structural change. 1. Microstate linear free energy relations, *Biochemistry 43*, 12048−12064.
41. Vickery, L., Nozawa, T., and Sauer, K. (1976) Magnetic circular dichroism studies of low-spin cytochromes. Temperature dependence and effects of axial coordination on the spectra of cytochrome *c* and cytochrome b_5, *J. Am. Chem. Soc. 98*, 351−357.
42. O'Connor, D. B., Goldbeck, R. A., Hazzard, J. H., Kliger, D. S., and Cusanovich, M. A. (1993) Time-resolved magnetic circular dichroism and absorption spectroscopy of CO photodissociation in cytochrome c_3 from *Desulfovibrio vulgaris*, *Biophys. J. 65*, 1718−1726.
43. Bevington, P. R., and Robinson, D. K. (1992) *Data Reduction and Error Analysis for the Physical Sciences*, McGraw-Hill, New York.
44. Shastry, M. C. R., and Roder, H. (1998) Evidence for barrier-limited folding kinetics on the microsecond timescale, *Nat. Struct. Biol. 5*, 385−392.
45. Hagen, S. J., and Eaton, W. A. (2000) Two-state expansion and collapse of a polypeptide, *J. Mol. Biol. 297*, 781−789.
46. Chen, E. F., Goldbeck, R. A., and Kliger, D. S. (2004) The earliest events in protein folding: a structural requirement for ultrafast folding in cytochrome *c*, *J. Am. Chem. Soc. 126*, 11175−11181.
47. Jacobson, H., and Stockmayer, W. H. (1950) Intramolecular reaction in polycondensations. I. The theory of linear systems, *J. Chem. Phys. 18*, 1600−1606.
48. Wang, J. C., and Davidson, N. (1966) On the probability of ring closure of lambda DNA, *J. Mol. Biol. 19*, 469−482.
49. Hagen, S. J., Hofrichter, J., and Eaton, W. A. (1997) Rate of intrachain diffusion of unfolded cytochrome *c*, *J. Phys. Chem. B 101*, 2352−2365.
50. Szabo, A., Schulten, K., and Schulten, Z. (1980) First passage time approach to diffusion controlled reactions, *J. Chem. Phys. 72*, 4350−4357.
51. Muthukrishnan, K., and Nall, B. T. (1991) Effective concentrations of amino acid side chains in an unfolded protein, *Biochemistry 30*, 4706−4710.
52. Thomas, Y. G., Goldbeck, R. A., and Kliger, D. S. (2000) Characterization of equilibrium intermediates in denaturant-induced unfolding of ferrous and ferric cytochromes *c* using magnetic circular dichroism, circular dichroism, and optical absorption spectroscopies, *Biopolymers 57*, 29−36.
53. Chen, E., Abel, C. J., and Kliger, D. S., unpublished results.
54. Lapidus, L. J., Eaton, W. A., and Hofrichter, J. (2000) Measuring the rate of intramolecular contact formation in polypeptides, *Proc. Natl. Acad. Sci. U.S.A. 97*, 7220−7225.
55. Kubelka, J., Hofrichter, J., and Eaton, W. A. (2004) The protein folding "speed limit", *Curr. Opin. Struct. Biol. 14*, 76−88.
56. Bieri, O., Wirz, J., Hellrung, B., Schutkowski, M., Drewello, M., and Kiefhaber, T. (1999) The speed limit for protein folding measured by triplet-triplet energy transfer, *Proc. Natl. Acad. Sci. U.S.A. 96*, 9597−9601.
57. Callender, R. H., Dyer, R. B., Gilmanshin, R., and Woodruff, W. H. (1998) Fast events in protein folding: the time evolution of primary processes, *Annu. Rev. Phys. Chem. 49*, 173−202.
58. Pascher, T. (2001) Temperature and driving force dependence of the folding rate of reduced horse heart cytochrome *c*, *Biochemistry 40*, 5812−5820.
59. Schwarz, G. (1965) On the kinetics of the helix-coil transition of polypeptides in solution, *J. Mol. Biol. 11*, 64−77.
60. Muñoz, V., and Eaton, W. A. (1999) A simple model for calculating the kinetics of protein folding from three-dimensional structures, *Proc. Natl. Acad. Sci. U.S.A. 96*, 11311−11316.
61. Portman, J. J., Takada, S., and Wolynes, P. G. (2001) Microscopic theory of protein folding rates. I. Fine structure of the free energy profile and folding routes from a variational approach, *J. Chem. Phys. 114*, 5069−5081.
62. Portman, J. J., Takada, S., and Wolynes, P. G. (2001) Microscopic theory of protein folding rates. II. Local reaction coordinates and chain dynamics, *J. Chem. Phys. 114*, 5082−5096.
63. Privalov, P. L. (1992) Physical basis of the stability of the folded conformations of proteins, in *Protein Folding* (Creighton, T. E., Ed.) pp 83−126, W. H. Freeman, New York.

BI0622930